Chapter 60
Coupled Modelling of the Failure and Tsunami of a Submarine Debris Avalanche Offshore Central New Zealand

Xiaoming Wang, Joshu Mountjoy, William L. Power, Emily M. Lane, and Christof Mueller

Abstract Evidence of previous submarine mass failures in the form of excavation scars has been widely documented in the Cook Strait Canyons of New Zealand. Recent bathymetry surveying has identified a well-defined submarine landslide scar and its associated debris deposit on the northern slope of southern Hikurangi Trough. The newly acquired multi-beam data allowed determination of the location and extent of the deposit, estimation of its volume, as well as reconstruction of both the pre-failure bathymetry and the initial state of the mass failure. A dynamically coupled two-layer model was used to numerically investigate this submarine debris avalanche and its resulting tsunami impact on the coasts of central New Zealand. The modeling results show a fairly good overall agreement with the observed debris deposition and also suggest that tsunami associated with the debris avalanche quite possibly inundated the coasts of central New Zealand, with maximum run-up elevations of between 3 and 5 m in several nearby locations.

60.1 Introduction

The Southern Hikurangi Margin is where the Pacific plate is obliquely subducting beneath the Australian plate at ~20 mm/year, transforming and colliding with the intra-continental Alpine Fault of South Island, New Zealand (Wallace et al. 2004). The abundant supply of sediment from rapidly rising mountains in association with strong ocean currents, active faults and several submarine canyon systems, provides an ideal set of circumstances favouring frequent occurrences of submarine mass

X. Wang (✉) • W.L. Power • C. Mueller
GNS Science, Lower Hutt, New Zealand
e-mail: x.wang@gns.cri.nz

J. Mountjoy
National Institute of Water and Atmospheric Research (NIWA), Wellington, New Zealand
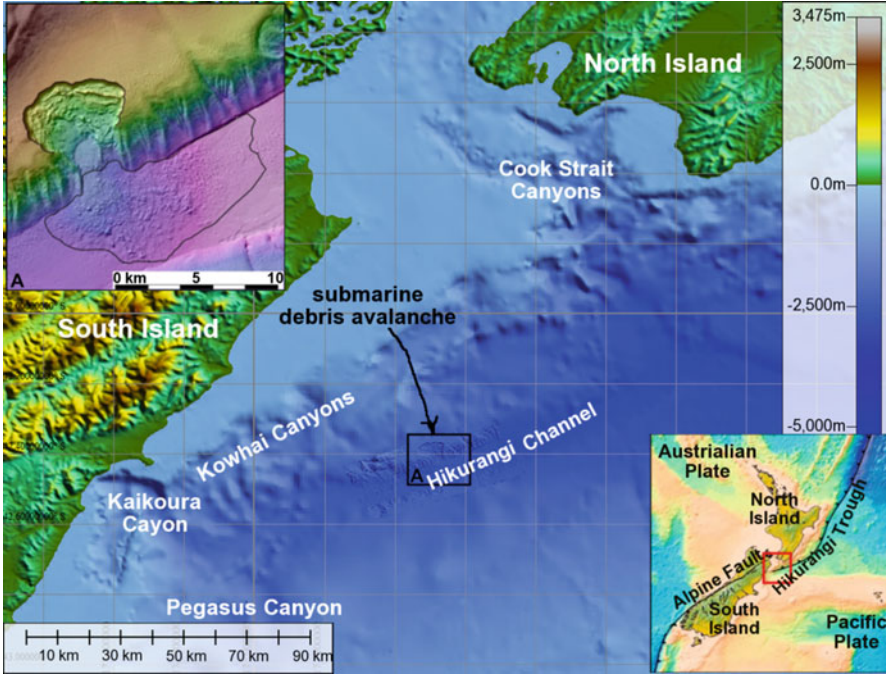
E.M. Lane
NIWA, Wellington, New Zealand

Fig. 60.1 Submarine canyons in central New Zealand. The submarine debris avalanche is shown in *A*. The *black contour* in *A* outlines the rough range of the debris deposit

failure (Fig. 60.1). Numerous past submarine mass failures have been identified in this region, especially in Cook Strait Canyons, Kaikoura Canyon and Pegasus Canyon (Lewis et al. 1998; Lewis and Pantin 2002; Mountjoy et al. 2009; Mitchelle et al. 2012), and these canyon systems are recognised to present potential landslide tsunami threat to the coast of central New Zealand.

Recently, a very well defined scar and its matching deposit were revealed in unprecedented detail on the southern side of the Hikurangi channel (Fig. 60.1a). Both the scar and the debris deposit remain well preserved, which provides a rare opportunity to study the failure and the tsunami impact. In this study, we investigated this submarine debris avalanche and the resulting tsunami with a dynamically coupled two-layer model. The model simultaneously calculates the debris avalanche and its resulting tsunami with a fully two-way coupled approach.

60.2 The Submarine Debris Avalanche

The submarine debris avalanche was identified off the northern apex of the southern Hikurangi Channel, lying about 2500 m under water (Fig. 60.1), among other submarine mass failures discovered during a recent Southern Hikurangi mapping
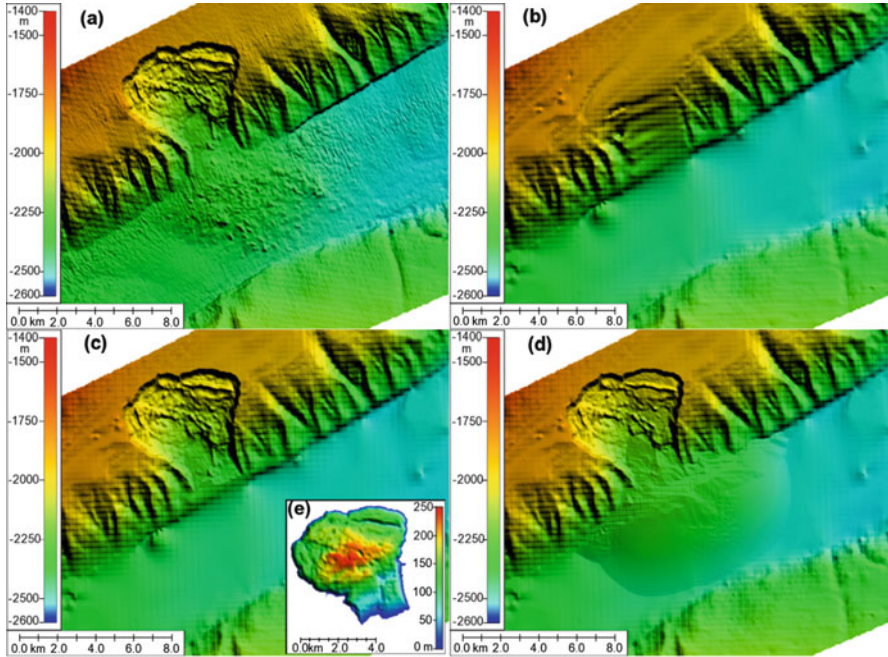
Fig. 60.2 (**a**) Post-failure bathymetry; (**b**) reconstructed pre-failure bathymetry; (**c**) bed surface of the failure; (**d**) computed post-failure bathymetry; and (**e**) initial debris thickness before failure

cruise (Mitchell et al. 2012). Onboard the RV a Kongsberg EM302 swath mapping instrument, operating at 30 kHz with 288 beams, provided a resolution better than in the previous imaging (Lewis and Pantin 2002). The high-resolution data indicates that the displaced debris remains well preserved on the channel floor, suggesting that it must have occurred within the timeframe of present geomorphology. The pristine status of the amphitheater-like scar and the matching deposit on the relatively flat floor allows outlining the range of debris deposition, restore the pre-failure bathymetry, and estimate the volume of the initial mass (Fig. 60.2). The initial mass was estimated as approximately 2.5 km^3, with a maximum thickness about 250 m and over 6.0 km wide (Fig. 60.2e).

Past studies suggest that the sediment in this region ranges from fine-grained sand to coarser granule sand and gravels (Lewis and Pantin 2002). The low cohesion of such material and the widespread debris deposition on the channel floor imply that the failure disintegrated and transformed into a debris avalanche after its initiation. But it is not clear where the failure started and what caused it. Due to its proximity to active faults, it is suspected that earthquake-induced strong ground shaking was likely the trigger.

60.3   Numerical Model and Modeling Results

Debris avalanche has often been modelled with depth-integrated equations, owing
to the fact that the thickness of debris flow is usually over one order-of-magnitude
smaller than its spatial scales (Jiang and LeBlond 1992). In particular, Heinrich
et al. (2001) and Kelfoun and Druitt (2005) solved these types of equations in a
topography-linked local coordinate system. This approach reduces difficulties in
solving vertically integrated equations over relatively steep terrains.

In this study, a fully-coupled two-layer model was proposed to study this
submarine debris avalanche and its consequent tsunami. The debris avalanche in
the lower layer serves as forcing boundaries for tsunami modeling in the upper
layer. For simplicity while remaining effectiveness, the thickness-averaged
Eq. (60.1), similar to those of Heinrich et al. (2001), were used to describe the
debris avalanche with granular flow assumption.

$$
\frac{\partial h}{\partial t} + \frac{\partial (hu_s)}{\partial \widetilde{x}} + \frac{\partial (hv_s)}{\partial \widetilde{y}} = 0
$$

$$
\frac{\partial (hu_s)}{\partial t} + \alpha \left[\frac{\partial (hu_s u_s)}{\partial \widetilde{x}} + \frac{\partial (hu_s v_s)}{\partial \widetilde{y}} \right] = khg\sin\theta_x - khg\cos\theta \frac{\partial h}{\partial \widetilde{x}} + f_{\widetilde{x}}
$$

$$
+ f\widetilde{x}' \frac{\partial (hv_s)}{\partial t} + \alpha \left[\frac{\partial (hv_s u_s)}{\partial \widetilde{x}} + \frac{\partial (hv_s v_s)}{\partial \widetilde{y}} \right]
$$

$$
= khg\sin\theta_y - khg\cos\theta \frac{\partial h}{\partial \widetilde{y}} + f_{\widetilde{y}} + f\widetilde{y}' \tag{60.1}
$$

in which h, u_s and v_s denote the slope-normal thickness and the velocity compo-
nents in slope-parallel directions $\widetilde{x}$ and $\widetilde{y}$, respectively; θ is hydrologic slope angle,
and $\theta_{\widetilde{x}}, \theta_{\widetilde{y}}$, are slope angles in $\widetilde{x}$ and $\widetilde{y}$; α relates to the over-thickness velocity
profile. In this study, $\alpha = 1.0$, assuming a uniform over-thickness velocity profile.
Parameter k reflects the effect of water. $k = 1.0$ for terrestrial avalanches and
$k = 1 - 1/\rho_s$ for submarine avalanches in which ρ_s is the density ratio of mass to
water. $\rho_s = 2.15$ was used here, which is an average of the values 1.85~2.45 found
in other studies. g = 9.801 m^2/s.

In Eq. (60.1), $f'_{\widetilde{x}}$ and $f'_{\widetilde{y}}$ are counter-components of top interface friction
determined from Eq. (60.4) which also introduce two-way momentum exchange
between (60.1) and (60.3). $f_{\widetilde{x}}$ and $f_{\widetilde{y}}$ are frictional force components, determined
from a Coulomb-type friction law commonly used for granular flow simulations as

$$
f_{\widetilde{x}} = khg \cos\theta \tan\varphi \left(u_s / \left| \vec{u}_s \right| \right), \quad f_{\widetilde{y}} = khg\cos\theta\tan\varphi \left(v_s / \left| \vec{u}_s \right| \right) \tag{60.2}
$$

where $\vec{u}_s = (u_s, v_s)$; φ is Coulomb friction angle, approximately encapsulating the
effects of basal and internal frictions. Without additional momentum input, debris

does not move over a slope less than this angle. $\varphi = 4.0°$ was adopted in this study, estimated from the repose angle of the debris deposit.

This debris avalanche model was further coupled with the depth-averaged Nonlinear Shallow Water Equation (NSWE) model in the well-established COMCOT simulation package (Wang and Power 2011) to simulate the resulting tsunami in the upper layer. In the Cartesian system (χ, y, z) with χ, y and z pointing eastward, northward and upward respectively, the NSWEs read

$$\frac{\partial H}{\partial t} + \frac{\partial P}{\partial x} + \frac{\partial Q}{\partial y} = 0$$
$$\frac{\partial P}{\partial t} + \frac{\partial P^2}{\partial x} + \frac{\partial (PQ)}{\partial y} + gH\frac{\partial z_w}{\partial x} + f_x = 0 \qquad (60.3)$$
$$\frac{\partial Q}{\partial t} + \frac{\partial (PQ)}{\partial x} + \frac{\partial Q^2}{\partial y} + gH\frac{\partial z_w}{\partial y} + f_y = 0$$

where H stands for the vertical thickness of water column, $H = z_w - z_s$, in which Z_w denotes water surface elevation and Z_s is the top surface of debris. $z_s = z_b + h/cos\theta$ where Z_b represents the bed surface where the debris moves (Fig. 60.2c), and h and θ are obtained from the debris avalanche model. $P = Hu_w$ and $Q = Hv_w$ represent volume flux components, and u_w and v_w are velocity components of tsunami in x and y, respectively.

In Eq. (60.3), f_x and f_y are friction components at the water bottom determined from Manning's formula in Eq. (60.4), based on the relative velocity between debris avalanche and tsunami. Manning's roughness $n = 0.015$ was chosen for the sandy/muddy floor in this study. The friction along the interface of avalanche and tsunami motions, updated at every time step, serves as a feedback mechanism of momentum exchange between the two processes.

$$f_x = gn^2H^{-1/3}(u_w - u_s cos\,\theta_x)\sqrt{(u_w - u_s cos\,\theta_x)^2 + (v_w - v_s cos\,\theta_y)^2}$$
$$f_y = gn^2H^{-1/3}(v_w - v_s cos\,\theta_y)\sqrt{(u_w - u_s cos\,\theta_x)^2 + (v_w - v_s cos\,\theta_y)^2} \qquad (60.4)$$

The modified explicit staggered leap-frog Finite Difference (FD) scheme in Wang and Liu (2011) together with Arakawa C-grids was implemented to solve the NSWEs for tsunami evolutions. One advantage of this scheme is that numerical dispersion, part of truncation errors in the discretized NSWEs, is manipulated to resemble the weak physical dispersion property of classic Boussinesq equations, with a high computational efficiency. This was used to account for the potential dispersion effect of the tsunami generated from the deep channel. Based on Watts et al. (2003), the characteristic wavelength of the tsunami with solid-block motion assumption was estimated about 10–15 times larger than the channel depth, i.e., weakly dispersive waves. The characteristic wavelength will be even longer for the fully deformable landslide in this case study.
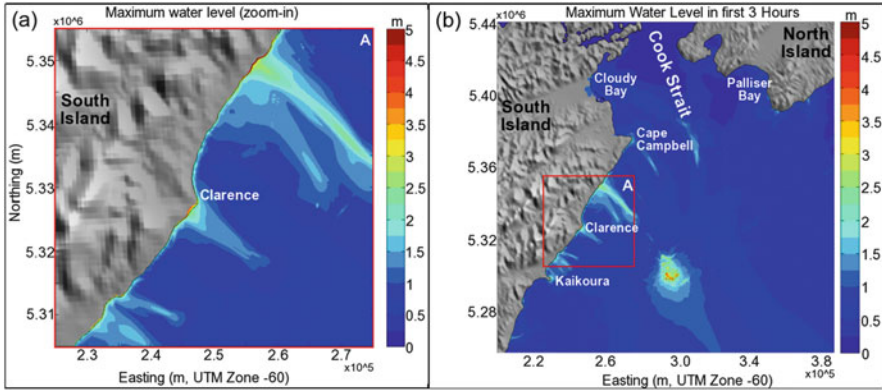
Fig. 60.3 (**a**) Computed max tsunami elevation near the coast (zoom-in view of box A); (**b**) Computed max tsunami elevation in central New Zealand

Equation (60.1) for avalanche-type motions were solved with the explicit upwind FD schemes proposed by Kelfoun and Druitt (2005), however with more general quadrilateral grids to discretize the terrain surface. The rectilinear grids in Heinrich et al. (2001) and in Kelfoun and Druitt (2005) are hardly achievable for complex terrains. The topography-linked quadrilateral grids were constructed by vertically projecting the horizontal Arakawa C-grids onto the topographical surface. Our tests indicated that this type of grid implementation allows easy coupling with the existing tsunami model, and the model also produces satisfactory agreements with analytical studies, e.g., those in Mangeney et al. (2000). One hundred-meter horizontal resolution was used in the simulation, enough to capture leading-order features of the debris avalanche and tsunami evolutions. In total, a 3-h duration of avalanche and tsunami was simulated to investigate the resulting tsunami impact on the coast of central New Zealand.

The computed final debris deposition and the maximum tsunami elevation are shown in Figs. 60.2d and 60.3, respectively. The computed post-failure bathymetry (Fig. 60.2d) reproduced the observation (Fig. 60.2a) fairly well, except for some details. Close comparisons reveal that the largest discrepancies over 25 m occur near the toe of the excavation scar and between the upper crown and bar-like scarp, probably due to inaccurate reconstruction of the bed surface (Fig. 60.2c). Without additional coring data, such reconstruction proves to be particularly challenging. Furthermore, in this simulation the entire initial mass was assumed to fail simultaneously at the beginning. In reality, the failure might start from one part then spread to other parts, e.g., in the type of a progressive or retrogressive failure.

Figure 60.4 shows the computed sequential snapshots of the debris avalanche with the assumption of simultaneous failure of the entire initial mass. The results suggest that in this failure scenario the most energetic process likely completed in the first 5–6 min, however the whole process might last over 10 min to reach the new equilibrium (Fig. 60.4). Tsunami might have been generated and affected most of the coasts of central New Zealand, with maximum elevations up to 3–5 m above
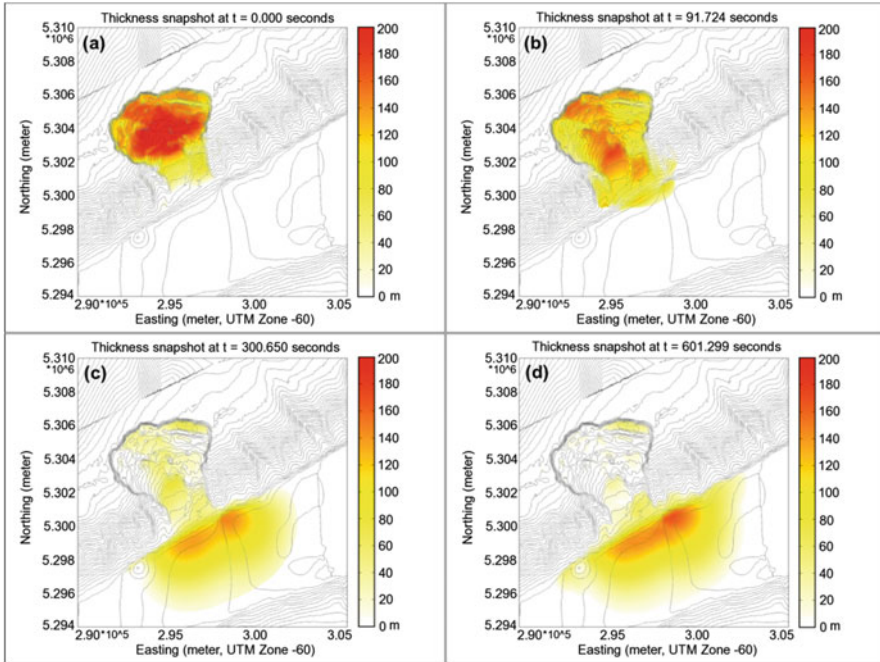
Fig. 60.4 Computed sequential snapshots of vertical thickness of debris at about (**a**) 0.0, (**b**) 1.5, (**c**) 5.0 and (**d**) 10.0 min into the simulation. *Grey lines* illustrate the bathymetry contours of the bed floor at a 20-m depth interval

ambient sea level in a few places from Kaikoura to Cape Campbell (Fig. 60.3). This estimate of the tsunami size is conservative, i.e., a worst case, because of the assumption that the failure started as a single large mass. Further investigation and modeling are required to improve our understanding of the pre-failure bathymetry, probable failure sequence and the characteristics of the resulting tsunami.

60.4 Conclusion

A well-defined submarine debris avalanche in the southern Hikurangi Channel was investigated to study its failure and the resulting tsunami impact on the coast of central New Zealand, using a fully coupled two-layer numerical model. Newly acquired high-resolution multi-beam data was used to reconstruct the pre-failure bathymetry and restore the initial condition of the mass failure. The numerical model generates a reasonable correspondence with the observed debris deposit caused by the failure, although it is recognized that this initial model requires further work and refinement. The modeling results also suggest that a related tsunami of moderate size may have been generated. If this was the case, it would

have affected the coasts of central New Zealand, with elevations up to 3–5 m above ambient water level in a few areas from Kaikoura to Cape Campbell.

The proposed model calculates debris avalanche and tsunami evolutions in a fully coupled two-layer system. The avalanche-type mass failure in the lower layer is computed with thickness-averaged equations in topography-linked coordinate system, serving as forcing boundaries for tsunami modeling in the upper water layer. Friction along the interface acts as a mechanism of momentum exchange between the two processes. This case study demonstrates that the coupled model can successfully model tsunamis by this type of mass failure.

References

Heinrich P, Piatensi A, Hebert H (2001) Numerical modelling of tsunami generation and propagation from submarine slumps: 1998 Papua New Guinea event. Geophys J Int 145:97–111

Jiang L, LeBlond PH (1992) The coupling of a submarine slide and the surface waves which it generates. J Geophys Res 97((C8) 12):731–744

Kelfoun K, Druitt TH (2005) Numerical modeling of the emplacement of Socompa rock avalanche. Chile J Geophys Res 110:B12202. doi:10.1029/2005JB003758

Lewis KB, Pantin HM (2002) Channel-axis, overbank and drift sediment waves in the southern Hikurangi Trough, New Zealand. Mar Geol 192:123–151

Lewis KB, Collott JY, Lallemand SE (1998) The dammed Hikurangi Trough: a channel-fed trench blocked b subducting seamounts and their wake avalanches (New Zealand-France GeodyNZ Project). Basin Res 10:441–468

Mangeney A, Heinrich P, Roche R (2000) Analytical solution for testing debris avalanche numerical models. Pure Appl Geophys 157:1081–1096

Michelle J, Mountjoy J, Barnes P (2012) OS20/20 southern Hikurangi voyage report prepared for land information NZ. NIWA client report no: WLG2012-21, May 2012

Mountjoy JJ, Barnes PM, Pettinga JR (2009) Morphostructure and evolution of submarine canyons across an active margin: cook strait sector of the Hikurangi Margin, New Zealand. Mar Geol 260(1–4):45–68

Wallace LM, Beavan J, McCaffrey R, Darby D (2004) Subduction zone coupling and tectonic block rotations in the North Island, New Zealand. J Geophys Res 109:B12406. doi:10.1029/2004JB003241

Wang X, Liu P (2011) An explicit finite difference model for simulating weakly nonlinear and weakly dispersive waves over slowly varying water depth. Coast Eng 58:173–183

Wang X, Power W (2011) COMCOT: a tsunami generation propagation and run-up model, GNS science report 2011/43, 129p

Watts P, Grilli ST, Kirby JT, Fryer GJ, Tappin DR (2003) Landslide tsunami case studies using a Boussinesq model and a fully nonlinear tsunami generation model. Nat Hazards Earth Syst Sci 3:391–402